Biosensors and Bioelectronics 294 (2026) 118199

Contents lists available at ScienceDirect

Biosensors and Bioelectronics

journal homepage: www.elsevier.com/locate/bios

Rapid detection of Staphylococcus aureus using a fluorescent PoC array for perioperative guidance for infection

Rossella Santonocito [a], Sofia Avnet [b], Nunzio Tuccitto [c], Nicolò Musso [d,e], Alessia Cavallaro [c], Michael Spinello [c], Maria Veronica Lipreri [a], Martina Ricceri [a], Ilenia Martina Pia Filannino [a], Ilaria Raimondi [a], Stefania Stefani [e,f], Nicola Baldini [a,b], Giuseppe Trusso Sfrazzetto [c,*]

[a] Biomedical Science, Technologies, and Nanobiotechnology Lab, IRCCS Istituto Ortopedico Rizzoli, Bologna, 40136, Italy
[b] Department of Biomedical and Neuromotor Sciences, University of Bologna, Bologna, 40138, Italy
[c] Department of Chemical Sciences, University of Catania, Viale A. Doria 6, Catania, 95100, Italy
[d] Faculty of Medicine and Surgery, "Kore" University of Enna, Contrada Santa Panasia, Enna, 94100, Italy
[e] A.I.D.A. - ADVANCED AND INNOVATIVE DIAGNOSTICS ACADEMY S.R.L, Via Santa Sofia 97, Torre Biologica, Catania, 95100, Italy
[f] Department of Biomedical and Biotechnological Sciences, University of Catania, Via Santa Sofia 97, Catania, 95123, Italy

ARTICLE INFO

Keywords:
Optical array
Point-of-care
Infections
Orthopaedic surgery

ABSTRACT

Culture and other conventional diagnostic tests are hindered in their practicality as they are time- and labour intensive to perform. Point-of-care (POC) are designed for rapid, on-site pathogen detection and are increasingly recognized as a crucial tool for timely clinical decisions, especially in clinical settings in which the collection of the correct specimen requires invasive procedures, helping in defining effective therapies and optimizing patient management, particularly in perioperative settings. Accurate and timely detection of bacterial infection is critical for defining effective therapies and optimizing patient management, particularly in perioperative settings. *Staphylococcus aureus*, a leading cause of periprosthetic joint infection, requires rapid and reliable detection in order to define proper surgical treatment. We present an innovative portable point-of-care (PoC) device based on a fluorescent sensor array for the direct detection of *S. aureus*, via its secretome, in biological fluids, without the need for sample pre-treatment or signal amplification, minimizing false positives. Experimentally trained on bacterial supernatants, the sensor array delivers results within 40 min, achieving a low detection limit (10^2 CFU/mL) and a high selectivity, effectively discriminating *S. aureus* from other Gram-positive and -negative species. With a cost of ~ € 5 per sample, this tool is suitable for clinical as well as decentralized settings. Preliminary evaluations in simulated synovial fluid further highlighted its potential in clinical settings.

1. Introduction

Deep infection associated with bone and joint implants are a challenging complication of orthopaedic procedures. Among the causative pathogens, *Staphylococcus aureus* is one of the most common pathogens, ranging from 0.7 % to nearly 2 % of cases, depending on the procedure and clinical setting. *S. aureus*, is also associated with the highest treatment failure rates. A key factor contributing to its persistence is its ability survive intracellularly in phagosomes or in the cytoplasm in immune and bone cells, including osteocytes (Kavanagh et al., 2018; Davis et al., 2022; Lew and Waldvogel, 2004; Tande et al., 2014; Fraunholz and Sinha, 2012; Zelmer et al., 2024; Häffner et al., 2020; Gimza and Cassat, 2021; Stracquadanio et al., 2021; Bongiorno et al., 2021). *S. aureus* accounts for approximately 35–48 % of culture-confirmed surgical site infections and is also a cause of post-surgery bloodstream infection. These infections can progress rapidly, leading to implant failure, systemic complications, and increased mortality. Recurrent and chronic infections, associated with treatment failure, occur in up to 46 % of cases. From what sad above, early detection of *S. aureus*, particularly in synovial fluid, is crucial for timely therapeutic intervention, which can reduce hospitalization, treatment costs, and mortality (Hardtstock et al., 2020). However, detecting subclinical or early-stage infections remains challenging due to the bacteria's ability to evade detection, the limitations of current

* Corresponding author.
E-mail address: giuseppe.trusso@unict.it (G. Trusso Sfrazzetto).

https://doi.org/10.1016/j.bios.2025.118199
Received 27 August 2025; Received in revised form 30 October 2025; Accepted 2 November 2025
Available online 7 November 2025

diagnostic methods, and the complex environment of bone and implant surfaces.

The main challenges include the low sensitivity of standard cultures, biofilm formation, the need for rapid, accurate, and low-cost diagnostic tools. Conventional methods, such as blood tests, imaging, Gram staining, culture-based techniques, and automated systems like MALDI-TOF, are the current standard but suffer from delayed results (48–72 h), suboptimal sensitivity, and an underestimation of infection prevalence by up to one-third. These limitations are exacerbated during preoperative screening in early-stage infections, when antibiotics have been administered (Vilén et al., 2021; Oviaño et al., 2018; Petrucca et al., 2020), bacterial loads are low, sampling is poor (Sulovari et al., 2021). To address these limitations, several emerging technologies have been proposed, including 16S rRNA sequencing, real-time PCR, digital PCR, flow cytometry, immunofluorescence imaging, and microfluidic platforms coupled with isothermal amplification (Chen et al., 2019; Zhao et al., 2018; Ivy et al., 2018). Each of these approaches offer distinct advantages and drawbacks. PCR- and sequencing-based workflows demonstrate high sensitivity, capable of detecting *S. aureus* DNA in culture-negative samples but require labor-intensive workflows and lengthy protocols. Digital PCR achieves ultra-low detection limits (~13 copies/μL) but demands costly instrumentation (Belanger et al., 2025). Immunofluorescence imaging and flow cytometry provide rapid results (under 30 min) but often lack species-level specificity (Dossou et al., 2022). Promising strategies include microfluidic devices combined with loop-mediated isothermal amplification (LAMP) or integrated capture-PCR modules, which can detect live bacteria at concentrations as low as 1–10 CFU/reaction within 75 min (Chen et al., 2017). However, most of these techniques, are frequently susceptible to false positives or environmental contamination due to their reliance on massive signal amplification systems. In addition, most of these systems remain at the prototype stage and require significant optimization for real-world use further limiting their practical application.

Optical sensor arrays have recently emerged as a versatile and effective platform for bacterial diagnostics (Yang and Zhang, 2023). These systems utilize cross-reactive fluorescent dyes or nanomaterials, arranged in miniaturized arrays to detect changes in fluorescence patterns, which are analysed using chemometric analysis or machine learning models. They offer rapid, label-free detection of multiple bacterial species within minutes, using only microliters of sample (Svechkarev et al., 2018). Importantly, combining multiplexing capability, low cost, portability, and field-deploy ability, these platforms are particularly well-suited for point-of-care (PoC) applications (Laliwala et al., 2022). Array-based sensors offer several advantages: *1)* the use of organic molecules as fluorescent probes provides enhanced stability; *2)* fluorometric detection, compared to colorimetric detection, allows multiplexing of different chromatic outputs in a single measurement (sensor array), facilitating high-throughput analysis with minimal sample volumes; and *3)* the possibility of training the sensor array using multivariate analysis and machine learning to build a robust calibration library and improve selectivity (Cavallaro et al., 2024). Advances in array design and analytical techniques have made these tools highly promising for biomedical applications, including precision medicine.

In this study, we propose a compact, low-cost PoC device based on a fluorescent sensor array capable of the rapid detection of the presence of *S. aureus* directly from the analysis of its secretome in complex biological samples. The system requires no sample pre-treatment or signal amplification, minimizing false positives. Detection is based on chemoselective interactions between immobilized probes and bacterial targets to generate species-specific fluorescence patterns. These are captured via optical fiber and processed using statistical recognition models. Our platform delivers results within 40 min, achieves a detection limit of 10^2 CFU/mL, and maintains a per-test cost of ~€ 5, making it suitable for both hospital and outpatient settings. We describe the design, optimization, and performance evaluation of the system, with focus on its ability to reliably discriminate *S. aureus* from other bacterial species in buffer and simulated synovial fluid. The innovation of our device lies in: *i*) Rapid, straightforward analysis, *ii*) Use of unprocessed samples, enabled by synthetic probe chemistry; *iii*) Low per-test cost; *iv*) High selectivity for the target analyte.

Rather than replacing conventional diagnostics, this system is intended to complement them, providing an early detection tool that can function at a stage when traditional methods are likely to miss emerging infections.

2. Materials and methods

Some of the 20 probes reported in Fig. 1 are known in literature (PBEP, OBEP, MBEP, PBP, OBP, MPB (Santonocito et al., 2023a,b), BDPy-di-NH_2 (Tuccitto et al., 2021), BDPy-di-EA (Santonocito et al., 2023a,b), BDPy-Ar-OH, BDPy-Ar, Naph-isopropyl (Cavallaro et al., 2024), Naph-di-EA (Puglisi et al., 2019), Porph-di-OH (Đorđević et al., 2016), while the Bodipy probes in which fluoride atoms are replaced with alkyl or hydroxyl groups were synthesized following the reactions shown in the Supplementary material in Scheme S2 (Crawford and Thompson, 2010; Smithen et al., 2012).

Multivariate Classification and Selectivity tests are reported in the Supplementary Materials.

2.1. Bacterial samples preparation

S. aureus strain was cultured in Tryptic Soy Broth (TSB; Oxoid, UK; CM0129B) at 37 °C under aerobic conditions. Bacteria were grown for approximately 4 h until reaching the exponential phase corresponding to a concentration of 10^8 CFU/mL, in accordance with the growth curve. From the exponential phase culture, serial dilutions in TSB were performed to obtain final bacterial concentrations ranging from 10^7 to 10^2 CFU/mL. Each diluted sample was centrifugated at 8000×*g* for 10 min at 4 °C to remove bacterial cells. The supernatants were filtered through 0.22 μm filters to eliminate any residual cells. As a negative control, a sample of sterile medium was processed in the same way and used as a blank to subtract the background of the medium. All samples were processed using the same procedure in accordance with the growth kinetics of each bacterial species.

2.2. Procedure for analysis

Analysis was performed on the six samples at different concentrations, from 10^2 to 10^7 CFU/mL. Three sensor arrays were exposed to each solution and the emission spectra before and after the exposure were acquired.

The contribution of Tryptic Soy Broth (TSB) medium was also registered. For statistical treatment, the following formula was applied: formula [Ia/Ib) $_{bacteria}$- (Ia/Ib) $_{TSB}$], where Ia is the emission of each probe after the exposure to analyte, $Ia_{\_TSB}$ is the emission of each probe after the exposure to TSB and Ib is the emission of each probe before the exposure to any analyte. In detail, Figures S2-S125 (in the Supplementary Materials) report the emission spectra of each probe (20 probes) in triplicate, following exposure of the analyte and the blank. The intensity values ($Ia_{bacteria/TSB}$, $Ib_{bacteria/TSB}$) are collected by optical fiber and processed by MATLAB. The code recognizes the probes automatically using the naming convention in the file name, and then with "sort" command they are sorted in ascendant order. To prevent erroneous overwriting, any pre-existing ".xlsx" files in the working directory are first deleted. All ".txt" files contained in the folder are imported in the scripts and are organized as two column files (wavelength and intensity). A median filter is applied to the intensity values to reduce noise, after which the peak intensity and its corresponding wavelength are extracted for each measurement.

For each probe and each condition, the three peaks obtained from the three repetitions are averaged to produce a single representative value.

Subsequently, two ratios are calculated for each probe:

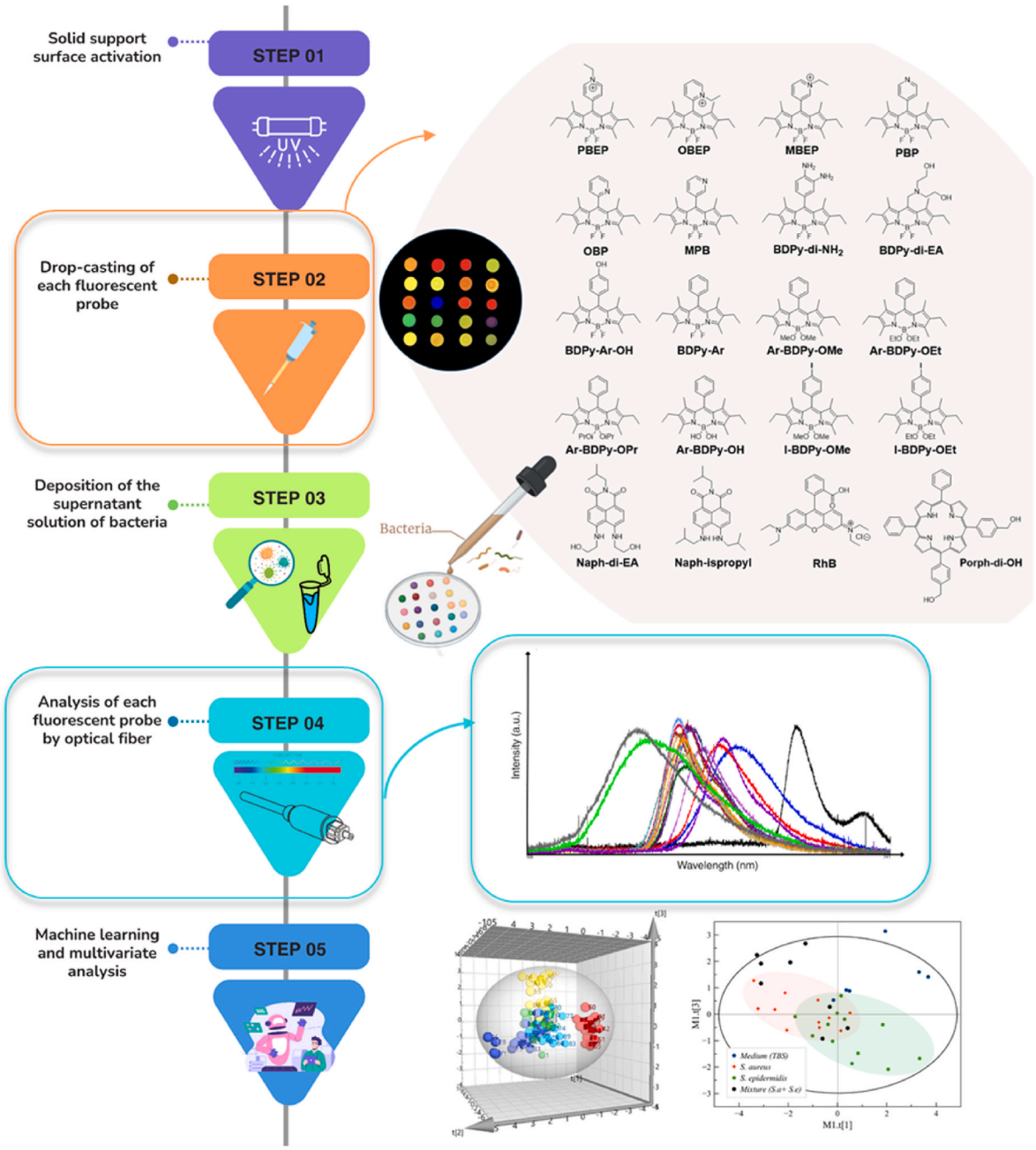

Fig. 1. Flowchart of the array analysis process.

- Ratio 1 ($value_{12}$): the ratio between the average intensity after exposure ($Ia_{bacteria}$) and the average intensity before exposure ($Ib_{bacteria}$).
- Ratio 2 ($value_{34}$): the ratio between the average intensity after exposure of TSB (Ia_{TSB}) and the average intensity before exposure of TSB (Ib_{TSB}).

The final output value for each probe is calculated as the difference between these two ratios.

The script generate:

- A plot for each probe, containing six subplots (comparing "before/after" for the bacteria and "before/after" for the TSB, for each of the three steps). Peaks are visualized for visual reference, and all spectra are displayed with filtered intensity values.
- A bar graph of the final values for all probes.
- Several ".xlsx" files summarizing the results, including peak intensities, peak wavelengths, and computed ratios.

This automated pipeline enables quantitative comparison between different experimental conditions and facilitates large-scale data handling.

2.3. Validation of the sensor for clinical use

To assess the potential clinical applicability of the array-based detection system, a sample of synovial fluid was artificially infected and analysed under the same conditions as the samples prepared in TSB to evaluate whether the biological matrix interfered with the analysis. A sample of human synovial fluid from single donor (Aurogene, Italy) was diluted 1:5 in Phosphate-Buffered Saline (PBS). *S. aureus* strain was cultured in TSB at 37 °C under aerobic conditions. Bacteria were grown

until reaching the exponential phase corresponding to a concentration of 10^8 CFU/mL, in accordance with the growth curve. From the exponential phase culture, serial dilutions in TSB were performed to obtain final bacterial concentrations ranging from 10^6 to 10^3 CFU/mL. Each diluted sample was centrifugated at 8000×*g* for 10 min at 4 °C to remove bacterial cells. The supernatants were filtered through 0.22 μm filters. The supernatants at different concentrations were diluted 1:10 in synovial fluid to obtain final concentrations ranging from 10^5 to 10^2 CFU/mL. A sample of equally diluted synovial fluid was used as a blank for analyses to subtract the background. For each solution, three sensor arrays also were employed, and the fluorescence measurements were taken following the procedure illustrated before.

For the PLS shown in Fig. 5, the following formula was used: [Ia/Ib) $_{\text{Aureus in synovial}}$- (Ia/Ib) $_{\text{synovial}}$], instead, for the PLS-DA was used for the first dataset: [Ia/Ib) $_{\text{synovial}}$- (Ia/Ib) $_{\text{TSB}}$] and [Ia/Ib) $_{\text{Aureus in synovial}}$ - (Ia/Ib) $_{\text{TSB}}$] for the second dataset.

3. Results and discussion

3.1. Design of the sensor array setup

The sensor is lightweight and compact and consists of 20 fluorescent synthetic probes. The advantage of using this type of probe is that the sensor array contains synthetic organic molecules, which are more stable compared to classical biomolecules (i.e., peptides of oligonucleotides used in PCR or ELISA methods), thus the effect of human fluids (e.g., blood or serum) to the stability of the sensor is not crucial for the analysis (Santonocito et al., 2025). In addition, the use of synthetic probes leads to the possibility to explore a wider concentration range respect to the classical point-of-care analytical methods. The synthetic fluorescent probes contain two different portions in the organic scaffold: a recognition site, able to interact by non-covalent interactions with the target analyte, and a fluorophore. Due to the huge number of metabolites released by bacteria, containing hydrophilic molecules as well as aromatic compounds, the non-covalent interactions should include hydrogen bonding, CH–π, π–π stacking, ion–dipole, and dipole–dipole forces. Unlike covalent sensing mechanisms, which typically produce a binary (on–off) response, non-covalent interactions generate more nuanced and analyte-dependent signal variations (Butera et al., 2021; Puglisi et al., 2018). In our array, we used different classes of chromophores, in particular rhodamines, Bodipys, naphthylamides and porphyrins, in order to cover a wide emission range, able to be detected by a sensitive and compact optical fiber device (Fan et al., 2019). The arrangement of each probe on the array is shown in Fig. 1.

Fluorescence emission from the probes in solid state was recorded through an optical fiber setup, upon excitation with a UV LED source (λ_{ex} = 365 nm), and detected by a CCD array (a silicon-based multichannel detector operating in the visible range). The optical fiber-based detection system was selected for its suitability in real-time analysis, offering key advantages such as low cost, mechanical flexibility, chemical resistance, and the ability to perform remote and multiplexed measurements on solid state. The complete setup includes: (i) a UV LED light source (λ_{ex} = 365 nm); (ii) an optical fiber guiding light to and from the sensor array; (iii) a CCD-based hyperspectral detector; and (iv) a computer for acquiring and displaying the fluorescence spectra.

The sensor array developed in this work is both easy to assemble and cost-effective. In fact, the overall cost per single analysis—including raw materials, solvents, reagents, and the time required for probe synthesis—is approximately 5 euros, which is significantly lower than that of most existing systems.

3.2. Staphylococcus aureus calibration

The procedure involves the preparation of three different arrays (in order to proceed with statistical analysis and evaluate the repeatability of the results by three independent measurements) with the 20 fluorescent probes deposited.

First, a polyamide solid support was pre-treated with exposure to a UV/O_3 lamp to increase its hydrophobicity and suitability for probe deposition. Next, 1.5 μL of each probe solution in ethanol (1 mM) was deposited. For each of the 20 fluorescent probes, the fluorescence was measured before and after exposure to the bacterial culture supernatant (TSB). The contribution of TSB (medium) must be subtracted from the analyte value; Fig. 1 shows the flowchart of the array analysis process. This step is crucial to eliminate the effect of different batches of TSB, provided by different laboratories,

We "trained" the array sensor to detect *S. aureus* at different concentrations, from 10^2 to 10^7 CFU/mL. The histogram shown in Fig. 2a represents the response of each probe following exposure to different concentrations of supernatant solutions of *S. aureus*, with positive and negative values representing the increase (enhancement) and decrease (quenching) of the emission intensity, respectively. In particular, the resulting normalised intensity is calculated using the formula ([(I_a/I_b) $_{\text{bacteria}}$- (I_a/I_b) $_{\text{TSB}}$]), where I_a is the intensity after the exposure of supernatant solution, I_b is the intensity before the exposure of the analyte, for the bacteria and TSB (medium) respectively, each intensity value is obtained as the average of three independent measures. The algorithm developed in MATLAB then allowed the spectra of the probes to be analysed iteratively and automatically form the working directory, and the values to be exported to Excel. To give an overview of the code, it is useful to perform the maximum value of each probe for each of the 4 steps with the corresponding wavelengths, the averages of the peaks for each probe in the three repetitions, and the final values calculated as the difference between the averages of the peaks of the first two steps and the averages of the peaks of the last two steps.

The normalised intensity values for each concentration were processed using multivariate statistical analysis. In particular, the PLS (Partial Least Squares) model was applied using 6 principal components (PC) to obtain an array response to the *S. aureus* bacterium, showing excellent linearity, with R^2 = 0.9992 (Fig. 2b, blue dots and red line). Notably, compared to the other POC devices based on biomolecules, our approach based on the use of synthetic organic probes shows the best results in terms of broad detection range (Atceken et al., 2023).

The training of the array was further validated by an independent dataset and by the analysis of an unknown concentration of *S. aureus*, supporting the robustness of the method. In particular, the independent dataset (orange triangles in Fig. 2b) was introduced as a validation set to assess the robustness of the PLS calibration model. Remarkably, these data points fall entirely within the calibration range, closely matching the expected trend and confirming the predictive reliability of the model, as evidenced by the high correlation (R^2 = 0.9956, green line).

To verify the possibility of analysing an unknown sample of *S. aureus*, we used PLS analysis. In particular, we used the PLS calibration model of *S. aureus* in TSB (which shows a good linear correlation between predicted and experimental concentrations) and added the data obtained from the sensor array for an unknown sample of *S. aureus* as a secondary test set (black star). In this case, in the absence of a reference concentration, the y-axis for this point was provided by the PLS model, while the x-axis was obtained from the linear fit equation in order to position the point on the line itself. From the graph shown in Fig. 2b, obtained through multivariate analysis, our array is able to quantify *S. aureus*, giving a concentration value of around 10^7 CFU/mL.

3.3. Selectivity tests

Selectivity plays a key role in ensuring reliable sensors performance under real-use conditions, especially to minimize false positives. We designed a series of experiments to evaluate the selectivity of the array towards *S. aureus* respect to other different bacterial species and, in addition, the effect of the matrix (TSB) on the performance of the sensor array and whether it could affect the identification and quantification of *S. aureus*. In particular we tested the other most frequent pathogens

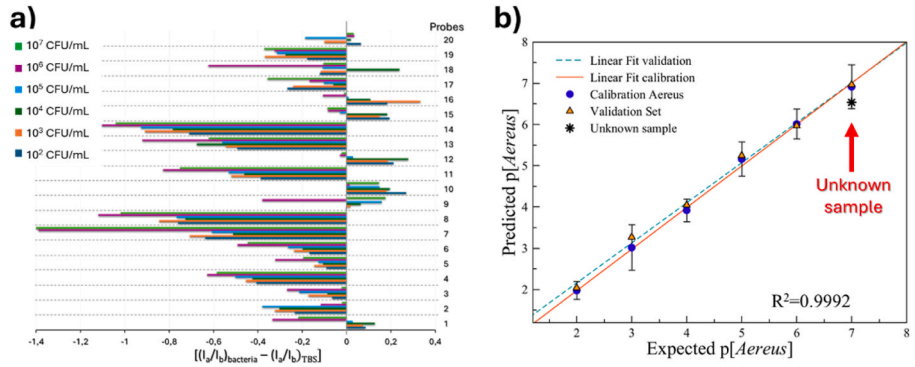

Fig. 2. a) Histogram represents the response of each probe following exposure to different concentrations of supernatant solutions of *S. aureus*. b) Expected *S. aureus* vs Predicted *S. aureus* calculated using PLS model with 6 PCs (blue dots) $R^2 = 0.9992$. Validation datasets is reported in orange triangles and unknown sample is reported in a black star ($R^2 = 0.9956$) (the error bars represent the standard deviations calculated on three replications). (For interpretation of the references to color in this figure legend, the reader is referred to the Web version of this article.)

associated with orthopaedic surgery (Li et al.,. 2018): i) *Staphylococcus epidermidis (S. epidermidis); ii) Escherichia coli (E. coli); iii) Pseudomonas aeruginosa (P. aeruginosa); iv) Enterococcus faecalis (E. faecalis).*

Fig. 3a–d shows the calibration of these bacteria in the range 10^2–10^7 CFU/mL. In particular, for each calibration performed on the supernatants of different bacteria, the PLS model was applied to obtain an array response to each bacteria species, showing excellent linearity, with $R^2 = 0.9992$ for *S. epidermidis, $R^2 = 0.9987$ for E. coli, $R^2 = 0.9983$*

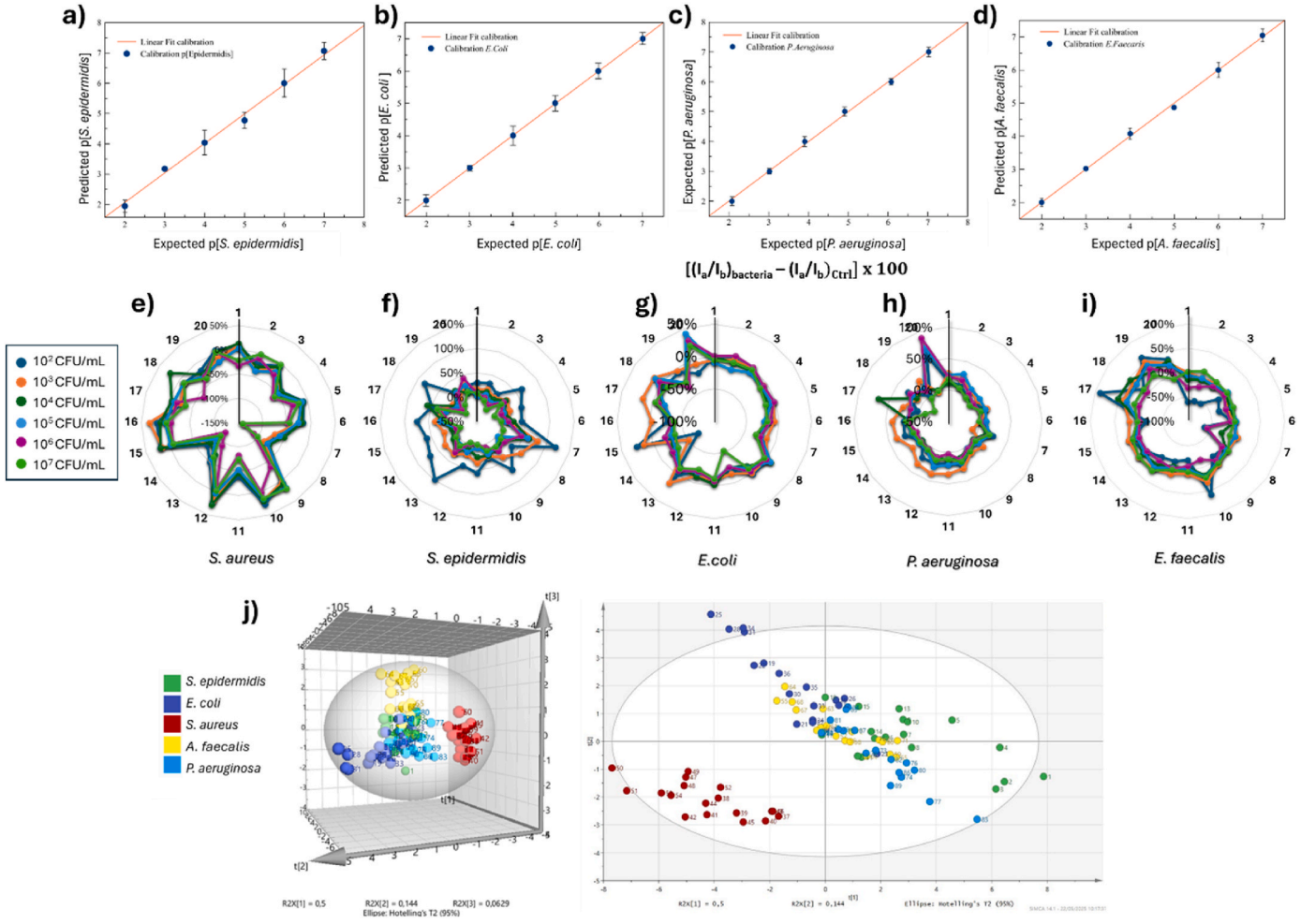

Fig. 3. Multivariate analysis: a) Expected *S. epidermidis* vs Predicted *S. epidermidis* calculated using PLS model with 5 PCs (blue dots) $R^2 = 0.9992$ (the error bars represent the standard deviations calculated on three replications); b) Expected *E. coli* vs Predicted *E. coli* calculated using PLS model with 6 PCs (blue dots) $R^2 = 0.9983$; c) Expected *P. aeruginosa* vs Predicted *P. aeruginosa* calculated using PLS model with 6 PCs (blue dots) $R^2 = 0.9987$; d) Expected *E. faecalis* vs Predicted *E. faecalis* calculated using PLS model with 7 PCs (blue dots) $R^2 = 0.9944$. (e–i): fingerprint of calibrations of four classes of bacterial species. j) Selectivity test by PLS-DA model, t1 vs t2 vs t3 scores plot. Ellipses represent T2 Hotelling at 0.95 confidence. (For interpretation of the references to color in this figure legend, the reader is referred to the Web version of this article.)

for P. aeruginosa and $R^2 = 0.9944$ for *E. faecalis* (Fig. 3a–d).

Fig. 3e–i represents the radar plots for each bacteria calibration. These radar plots report the emission change of each probe (from 1 to 20 in circular position) upon different bacteria concentrations. The resulting normalised intensity is calculated using the formula given above ($[(I_a/I_b)_{bacteria} - (I_a/I_b)_{TSB} \times 100]$). In particular, radar plots reported in Fig. 3e–i demonstrated that each bacterial species and concentration level generates a distinct radar plot profile, in terms of different shapes at different concentrations and different bacteria, resembling a unique fingerprint, highlighting the sensor array's ability not only to detect different bacterial strains but also to discriminate among them across the tested concentration range (10^2–10^7 CFU/mL). This is further supported by the PLS-DA (Partial Least Squares Discriminant Analysis) analysis (see Fig. 3j), in which a hierarchical clustering revealed clear identification of *S. aureus* respect to the other bacteria tested.

From PLS models, Very Important Parameters (VIPs) of the array response to each bacterium were obtained, to understand which probes are significant in the fluorescence response (see Supplementary Material, Figure S128–S132). As reported in Figure S1 (see Supplementary Material), BDPy-di-EA, BDPy-Ar, Ar-BDPy-OPr and I-BDPy-OCH_3 show the highest weight in the array response towards bacteria tested. Due to the huge number of metabolites released by these bacteria, probably the possibility to exploit π−π interactions between these probes and the metabolites is the driving force of the recognition process. We note that in our system, the recognition of bacteria is not based on the selective detection of a single molecular biomarker, but rather on the collective response to the wide array of metabolites released by the bacteria into the surrounding medium.

Indeed, bacterial supernatants are chemically complex mixtures containing dozens of metabolites with diverse structures and functionalities—including peptides, amines, organic acids, surfactants, and redox-active molecules. Most of these contains hydrophilic groups, able to perform hydrogen bonds. Attempting to selectively target only a few of these compounds would necessarily lead to a loss of selectivity, as other co-existing species could interfere or be missed entirely. To address this, we employ an array-based empirical sensing strategy. The 20 fluorescent dyes used in our platform were selected to cover a broad spectrum of chemical reactivities and photophysical behaviours, including sensitivity to polarity, pH, redox potential, hydrogen bonding, and π–π interactions. As a result, each probe responds differently—some with fluorescence enhancement, others with quenching—depending on the specific composition of the supernatant. This diversity in response creates a unique "fingerprint" for each bacterial species. This approach, while empirical in nature, is widely recognized and validated in the field of chemical sensing (Cavallaro et al., 2024; Li and Suslick, 2020; Santonocito et al., 2025; Santonocito et al., 2023a,b), and provides a robust framework for developing rapid and low-cost diagnostic tools without requiring detailed a priori knowledge of the individual chemical components in the sample.

Then, we validated the ability of the sensor array to recognize *S. aureus* and *S. epidermidis* in complex mixtures, performing unsupervised multivariate analysis by PLS-DA. In particular, we prepared four different mixtures of *S. aureus* and *S. epidermidis* (duplicated in this analysis), at different concentration values (mixture 1–4, see Materials and Method section for details). The primary dataset included three distinct classes: culture medium (TSB), *S. aureus*, and *S. epidermidis*. These were clearly separated by the PLS-DA model with 100 % classification accuracy (see Table S1 in the Supplementary Material for details). As a secondary dataset, we introduced sensor responses obtained from the four mixture samples. As shown in Fig. 4, the PLS-DA scores of the mixtures (black stars) are clearly located in a plot region separated from the culture medium cluster (TSB ellipses in Fig. 4). Furthermore, the mixtures containing mainly *S. aureus* (mixtures 1 and 2) are located in the plot region of pure *S. aureus* (red ellipses in Fig. 4), as well as the mixtures containing mainly *S. epidermidis* are located in the plot region of pure *S. epidermidis* (green ellipses in Fig. 4). This indicates that, even

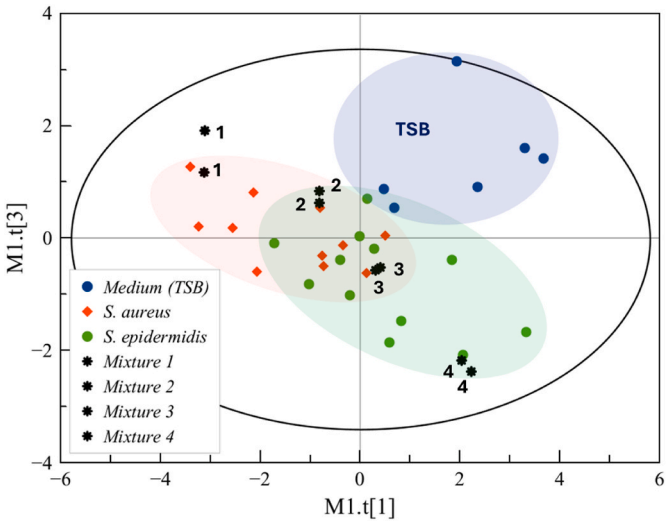

Fig. 4. PLS-DA model, t1 vs t3 scores plot. Ellipses represent T2 Hotelling at 0.95 confidence. 2D dots represent data obtained from calibration of *S. aureus* (red), *S. epidermidis* (green) and TSB (blue). The black stars represent data obtained from mixtures of *S. aureus* and *S. epidermidis*. Coloured ellipses are placed to help the eyes of the reader. (For interpretation of the references to color in this figure legend, the reader is referred to the Web version of this article.)

in the presence of complex bacterial mixtures, the sensor array successfully detects signatures indicative of bacterial presence. These results demonstrate the capability of our sensor array to qualitatively identify bacterial contamination, even in polymicrobial samples.

3.4. *S. aureus* sensing in simulated synovial fluid

To assess the potential of the sensor for clinical use in detecting bacterial infections during surgical procedures, a synovial fluid sample was prepared, diluted 1:5, and spiked with *Staphylococcus aureus* supernatants at concentrations of 10^2, 10^3, 10^4, and 10^5 CFU/mL, respectively. The contaminated samples were deposited onto the sensor array following the procedure previously described. Synovial fluid is an important preoperative sample for diagnostic testing, and it is usually collected via preoperative or intraoperative joint puncture. These samples are then used for microbiological culture and conventional real-time PCR testing (Yang et al., 2021).

Firstly, we calibrated our array for *S. aureus* in a simulated synovial fluid, in the range 10^2–10^5 CFU/mL, to demonstrate that this bacterium can be detected and quantified also in a simulated real sample. We also used uncontaminated (healthy) synovial fluid samples as control experiments. A PLS model was firstly applied to linearize the sensor responses, demonstrating that the quantification of *S. aureus* can be performed also in simulated synovia. Then, PLS-DA was applied to enable discrimination between healthy (red stars dots in Fig. 5) and contaminated synovial fluid samples (blue and green dots in Fig. 5). In particular, these results demonstrate that our array is able to detect *S. aureus* both in simulated synovial fluid (green dots) and in TSB medium (blue dots).

Several advanced laboratory techniques have been explored for the detection of bacterial infections in the synovial fluid, each with distinct advantages and limitations in terms of sensitivity, time-to-result, and clinical applicability. Molecular techniques such as 16S rRNA sequencing (Chen et al., 2019; Zhao et al., 2018) and metagenomic analysis (Ivy et al., 2018) offer excellent sensitivity but require 2–3 days to complete, making them unsuitable for rapid diagnostics. Systems based on digital PCR (Chen et al., 2017) and multiplexed panels like BIOFIRE (Esteban et al., 2023) provide faster results (1–3 h) with high

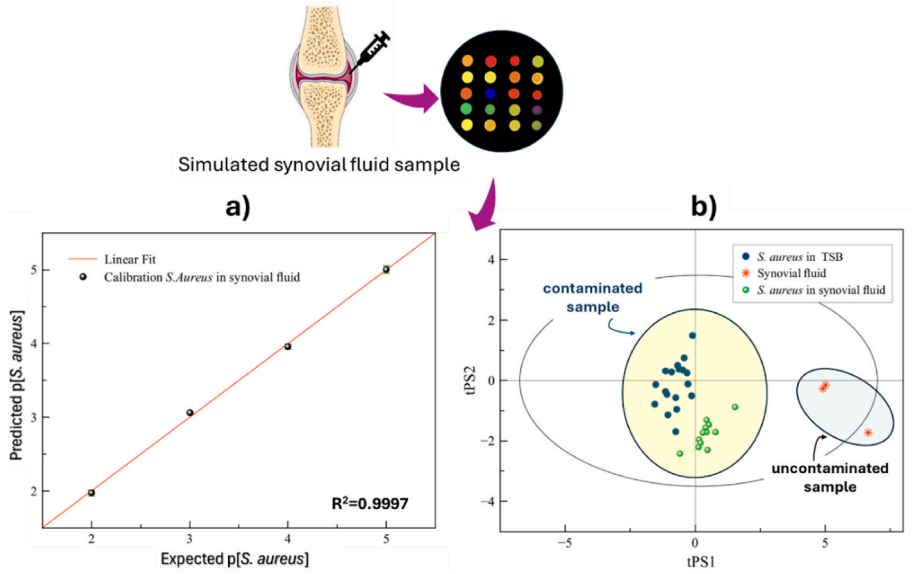

Fig. 5. a) Expected *S. aureus* in synovial fluid vs Predicted *S. aureus* in synovial fluid calculated using PLS model with 4 PCs (blue dots) $R^2 = 0.9997$ (the error bars represent the standard deviations calculated on three replications); b) PLS-DA model, t1 vs t2 scores plot. Ellipses represent T2 Hotelling at 0.95 confidence. 2D dots represent data obtained from calibration of S. aureus in TSB (blue dots), Synovial fluid (red stars), S. aureus in synovial fluid (green dots). Coloured ellipses are placed to help the eyes of the reader. (For interpretation of the references to color in this figure legend, the reader is referred to the Web version of this article.)

sensitivity, although they depend on complex instrumentation and elevated costs per test. Among the most effective platforms in terms of both speed and sensitivity are microfluidic devices employing EMA-LAMP or integrated capture-PCR modules (Ivy et al., 2018; Chen et al., 2017; Chang et al., 2014, 2015), which achieve detection limits down to 1–10 CFU/mL and complete analyses in under 90 min.

4. Conclusions

The experimental system proposed in this work falls within this latter category of advanced microfluidic PoC devices. It delivers quantitative results in less than 40 min, with a limit of detection of 10^2 CFU/mL and offers robust discrimination between *S. aureus* and other bacterial species. Furthermore, by analysing the secretum of the bacteria and by avoiding the amplification of the signal for the detection, it potentially minimizes the occurrence of false positive samples. Importantly, the cost per test is approximately 5 euros, significantly lower than that of most reported systems. Unlike conventional molecular diagnostics, our device does not require nucleic acid extraction or enzymatic amplification, relying instead on a chemometric interpretation of fluorescence patterns generated by a cross-reactive probe array.

This strategy combines the strengths of array-based sensing—such as pattern recognition, multiplexing, and adaptability—with the practical needs of clinical environments, offering a compelling balance of speed, sensitivity, specificity, and cost-efficiency. While the system does not currently provide species-level identification beyond trained targets, its simplicity, scalability, and low operational cost make it an attractive candidate for decentralized or rapid triage applications. One limitation of the present setup is the possibility to perform quantitative analyses in mixtures of bacteria. However, we believe that the increasing of the number of probes into the array can solve this problem, leading to higher selectivity.

Building on the promising results obtained with the fluorescent sensor array, future developments will focus on the integration of the sensing platform into a microfluidic chip. This transition will enable automated handling of small volumes, standardized sample preconditioning, and controlled delivery of reagents to the sensor surface. A microfluidic configuration would also allow the entire analysis—from sample introduction to data acquisition—to be carried out in a closed, compact, and disposable device, minimizing contamination risk and user intervention. Additionally, multiplexed microchannel designs could support parallel detection of multiple pathogens in synovial fluid, enhancing the diagnostic power of the system. Furthermore, the reducing dimensions lead to the possibility to increase the number of probes into the array, leading to higher selectivity and a wider range of applications. Coupling the microfluidic platform with smartphone-based optical readout and wireless data processing would further pave the way for the deployment of a truly portable, user-friendly, and low-cost diagnostic tool suitable for bedside or decentralized clinical applications. Current efforts are directed toward the prototyping of such devices using polymer-based fabrication techniques and their validation on real clinical samples.

CRediT authorship contribution statement

Rossella Santonocito: Writing – original draft, Validation, Investigation. **Sofia Avnet:** Validation. **Nunzio Tuccitto:** Validation. **Nicolò Musso:** Validation. **Alessia Cavallaro:** Investigation. **Michael Spinello:** Investigation. **Maria Veronica Lipreri:** Investigation. **Martina Ricceri:** Investigation. **Ilenia Martina Pia Filannino:** Investigation. **Ilaria Raimondi:** Formal analysis. **Stefania Stefani:** Conceptualization. **Nicola Baldini:** Conceptualization. **Giuseppe Trusso Sfrazzetto:** Writing – original draft, Supervision, Conceptualization.

Declaration of competing interest

The authors declare that they have no known competing financial interests or personal relationships that could have appeared to influence the work reported in this paper.

Acknowledgment

This research was funded by the European Union (NextGeneration EU) through the MUR-PNRR project SAMOTHRACE (ECS00000022). G. T.S and N.T. thank the EU project EmergeNow for the inspiration to develop a multi-sensing device.

Appendix A. Supplementary data

Supplementary data to this article can be found online at https://doi.org/10.1016/j.bios.2025.118199.

Data availability

Data will be made available on request.

References

Atceken, N., Alseed, M.M., Dabbagh, S.R., Yetisen, A.K., Tasoglu, S., 2023. Adv. Eng. Mater. 25, 2201174. https://doi.org/10.1002/adem.202201174.

Belanger, C.R., Locher, K., Velapatino, B., Charles, M.K., 2025. Diagn. Microbiol. Infect. Dis. 112, 116749. https://doi.org/10.1016/j.diagmicrobio.2025.116749.

Bongiorno, D., Musso, N., Caruso, G., Lazzaro, L.M., Caraci, F., Stefani, S., Campanile, F., 2021. Microbiologyopen 10, e1178. https://doi.org/10.1002/mbo3.1178.

Butera, E., Zammataro, A., Pappalardo, A., Trusso Sfrazzetto, G., 2021. ChemPlusChem 86, 681–695. https://doi.org/10.1002/cplu.202100071.

Cavallaro, A., Santonocito, R., Puglisi, R., Pappalardo, A., La Spada, F., Parlascino, R., Riolo, M., Cacciola, S.O., Tuccitto, N., Trusso Sfrazzetto, G., 2024. Chem. Commun. 60, 13702–13705. https://doi.org/10.1039/D4CC04700A.

Chang, W.-H., Wang, C.-H., Lin, C.-L., Wu, J.-J., Lee, M.S., Lee, G.-B., 2015. Biosens. Bioelectron. 66, 148–154. https://doi.org/10.1016/j.bios.2014.11.006.

Chang, W.-H., Wang, C.-H., Yang, S.-Y., Lin, Y.-C., Wu, J.-J., Lee, M.S., Lee, G.-B., 2014. Lab Chip 14, 3376–3384. https://doi.org/10.1039/c4lc00471j.

Chen, M.-F., Chang, C.-H., Chiang-Ni, C., Hsieh, P.-H., Shih, H.-N., Ueng, S.W.N., Chang, Y., 2019. Bone Joint Res. 8, 367–377. https://doi.org/10.1302/2046-3758.88.bjr-2019-0003.r2.

Chen, S.-L., Chang, W.-H., Wang, C.-H., You, H.-L., Wu, J.-J., Liu, T.-H., Lee, M.S., Lee, G.-B., 2017. Microfuid Nanofuid, vol. 21, p. 87. https://doi.org/10.1007/s10404-017-1913-8.

Crawford, S.M., Thompson, A., 2010. Org. Lett. 12, 1424–1427. https://doi.org/10.1021/ol902908j.

Davis, J.S., Metcalf, S., Clark, B., Robinson, J.O., Huggan, P., Luey, C., McBride, S., Aboltins, C., Nelson, R., Campbell, D., et al., 2022. Open Forum Infect. Dis. 9 (3). https://doi.org/10.1093/ofid/ofac048 ofac048.

Đorđević, L., Marangoni, T., De Leo, F., Papagiannouli, I., Aloukos, P., Couris, S., Pavoni, E., Monti, F., Armaroli, N., Prato, M., Bonifazi, D., 2016. Phys. Chem. Chem. Phys. 18, 11858–11868. https://doi.org/10.1039/C5CP06055A.

Dossou, N., Gaubert, I., Moriceau, C., Cornet, E., le Hello, S., Malandain, D., 2022. Microbiol. Spectr. 10, e01830. https://doi.org/10.1128/spectrum.01830-21, 21.

Esteban, J., Salar-Vidal, L., Schmitt, B.H., Waggoner, A., Laurent, F., Abad, L., Bauer, T. W., Mazariegos, I., Balada-Llasat, J.-M., Horn, J., Wolk, D.M., Jefferis, A., Hermans, M., Verhoofstad, I., Butler-Wu, S.M., Umali-Wilcox, M., Murphy, C., Cabrera, B., Craft, D., von Bredow, B., Leber, A., Everhart, K., Dien Bard, J., Ibarra Flores, I., Daly, J., Barr, R., Holmberg, K., Graue, C., Kensinger, B.J., 2023. Clin. Microbiol. 61, 1–13. https://doi.org/10.1128/jcm.00357-23.

Fan, Y.Z., Tang, Q., Liu, S.G., Yang, Y.Z., Ju, Y.G., Xiao, N., Luo, H.Q., Li, N.B., 2019. Appl. Surf. Sci. 492, 550. https://doi.org/10.1016/j.apsusc.2019.06.224.

Fraunholz, M., Sinha, B., 2012. Front. Cell. Infect. Microbiol. 2, 43. https://doi.org/10.3389/fcimb.2012.00043.

Gimza, B.D., Cassat, J.E., 2021. Front. Immunol. 12, 638085. https://doi.org/10.3389/fimmu.2021.638085.

Häffner, N., Bär, J., Dengler Haunreiter, V., Mairpady, Shambat S., Seidl, K., Crosby, H. A., Horswill, A.R., Zinkernagel, A.S., 2020. Front. Microbiol. 11, 1415. https://doi.org/10.3389/fmicb.2020.01415.

Hardtstock, F., Heinrich, K., Wilke, T., Mueller, S., Yu, H., 2020. BMC Infect. Dis. 19, 233. https://doi.org/10.1186/s12885-020-06738-z.

Ivy, M.I., Thoendel, M.J., Jeraldo, P.R., Greenwood-Quaintance, K.E., Hanssen, A.D., Abdel, M.P., Chia, N., Yao, J.Z., Tande, A.J., Mandrekar, J.N., Patel, R., 2018. J. Clin. Microbiol. 56, e00402–e00418. https://doi.org/10.1128/jcm.00402-18.

Kavanagh, N., Ryan, E.J., Widaa, A., Sexton, G., Fennell, J., O'Rourke, S., Cahill, K.C., Kearney, C.J., O'Brien, F.J., Kerrigan, S.W., 2018. Clin. Microbiol. Rev. 31, 1–25. https://doi.org/10.1128/CMR.00084-17.

Laliwala, A., Svechkarev, D., Sadykov, M.R., Endres, J., Bayles, K.W., Mohs, A.M., 2022. Anal. Chem. 94, 2615–2624. https://doi.org/10.1021/acs.analchem.1c05021.

Lew, D.P., Waldvogel, F.A., 2004. Lancet 364, 369–379. https://doi.org/10.1016/S0140-6736(04)16727-5.

Li, Z., Suslick, K.S., 2020. Acc. Chem. Res. 54, 950–960. https://doi.org/10.1021/acs.accounts.0c00671.

Li, B., Webster, T.J., 2018. J. Orthop. Res. 36, 22–32. https://doi.org/10.1002/jor.23656.

Oviaño, M., Rodríguez-Sánchez, B., Gómara, M., Alcalá, L., Zvezdanova, E., Ruíz, A., Velasco, D., Gude, M.J., Bouza, E., Bou, G., 2018. Clin. Microbiol. Infect. 24, 624–629. https://doi.org/10.1016/j.cmi.2017.09.010.

Petrucca, A., Santino, I., Gentile, G., Mazza, D., Viglietta, E., Iorio, R., Simmaco, M., Ferretti, A., Borro, M., 2020. Rapid Commun. Mass Spectrom. 34, 8791. https://publons.com/publon/10.1002/rcm.8791.

Puglisi, R., Pappalardo, A., Gulino, A., Trusso Sfrazzetto, G., 2019. ACS Omega 4, 7550–7555. https://doi.org/10.1021/acsomega.9b00502.

Puglisi, R., Pappalardo, A., Gulino, A., Trusso Sfrazzetto, G., 2018. Chem. Commun. 54, 11156–11159. https://doi.org/10.1039/C8CC06425C.

Santonocito, R., Cavallaro, A., Pappalardo, A., Puglisi, R., Marano, A., Andolina, M., Tuccitto, N., Trusso Sfrazzetto, G., 2025. Biosens. Bioelectron. 270, 116986. https://doi.org/10.1016/j.bios.2024.116986.

Santonocito, R., Cavallaro, A., Puglisi, R., Intravaia, M., Toscano, R.M., Pappalardo, A., Trusso Sfrazzetto, G., 2023a. Curr. Org. Chem. 27, 876–882. https://doi.org/10.3390/chemosensors11090503.

Santonocito, R., Spina, M., Puglisi, R., Pappalardo, A., Tuccitto, N., Trusso Sfrazzetto, G., 2023b. Chemosensors 11, 503. https://doi.org/10.3390/chemosensors11090503.

Smithen, D.A., Baker, A.E.G., Offman, M., Crawford, S.M., Cameron, T.S., Thompson, A., 2012. J. Org. Chem. 77, 3439–3453. https://doi.org/10.1021/jo3002003.

Stracquadanio, S., Musso, N., Costantino, A., Lazzaro, L.M., Stefani, S., Bongiorno, D., 2021. Pathogens 10, 239. https://doi.org/10.3390/pathogens10020239.

Sulovari, A., Ninomiya, M.J., Beck, C.A., Ricciardi, B.F., Ketonis, C., Mesfin, A., Kaplan, N.B., Soin, S.P., McDowell, S.M., Mahmood, B., Daiss, J.L., Schwarz, E.M., Oh, I., 2021. J. Orthop. Res. 39, 2141–2150. https://doi.org/10.1002/jor.24935.

Svechkarev, D., Sadykov, M.R., Bayles, K.W., Mohs, A.M., 2018. ACS Sens. 3, 700. https://doi.org/10.1021/acssensors.8b00025.

Tande, A.J., Osmon, D.R., Greenwood-Quaintance, K.E., Mabry, T.M., Hanssen, A.D., Patel, R., 2014. Am. Soc. Microbiol. 5, e01910–14. https://doi.org/10.1128/mBio.01910-14.

Tuccitto, N., Catania, G., Pappalardo, A., Trusso Sfrazzetto, G., 2021. Chem. Eur J. 27, 13715–13718. https://doi.org/10.1002/chem.202102094.

Vilén, A., Nilson, B., Petersson, A.C., Cigut, M., Nielsen, C., Ström, H., 2021. Acta Vet. Scand. 63, 34. https://doi.org/10.1186/s13028-021-00599-7.

Yang, C., Zhang, H., 2023. Microchim. Acta 190, 451. https://doi.org/10.1007/s00604-023-06021-5.

Yang, F., Choe, H., Kobayashi, N., Tezuka, T., Oba, M., Miyamae, Y., Morita, A., Abe, K., Inaba, Y., 2021. J. Orthop. Res. 39, 348–355. https://doi.org/10.1002/jor.24959.

Zelmer, A.R., Yang, D., Gunn, N.J., Solomon, L.B., Nelson, R., Kidd, S.P., Richter, K., Atkins, G.J., 2024. Antimicrob. Agents Chemother. 68 (10), e00808-24. https://doi.org/10.1128/aac.00808-24, 24.

Zhao, Y., Chen, B., Li, S., Yang, L., Zhu, D., Wang, Y., Wang, H., Wang, T., Shi, B., Gai, Z., Yang, J., Heng, X., Yang, J., Zhang, L., 2018. Sci. Rep. 8, 14305. https://doi.org/10.1038/s41598-018-32675-w.